Spectroscopy of disordered low-field sites in Cr^{3+}: Mullite glass ceramic

Robert Knutson,* Huimin Liu, and W. M. Yen*
Department of Physics and Astronomy, The University of Georgia, Athens, Georgia 30602

T. V. Morgan
Center for Metalloenzyme Studies, Department of Chemistry, The University of Georgia, Athens, Georgia 30602
(Received 24 October 1988; revised manuscript received 10 March 1989)

In this article we present results of optical and ESR studies that have allowed us to study the behavior of Cr^{3+} at disordered low-field sites within a mullite ceramic host. The results indicate that the existence of these low-field ions, which are likely at sites in regions of disorder, accounts for most of the spectroscopic anomalies previously noted in these materials. Furthermore, energy transfer from ordered high-field to disordered low-field ions is observed. The resulting complex spectra are deconvoluted by means of the recently developed technique of saturation-resolved fluorescence spectroscopy.

I. INTRODUCTION

The mullite glass ceramics developed recently by Corning Glass Works are part of a promising new class of high-crystal-field amorphous materials. Originally developed for luminescent solar converter applications, they have also received attention as solid-state laser materials.[1] Because they contain both ordered and disordered regions within their structure, they provide systems with which to study the order to disorder interface and energy-transfer dynamics.

Mullite is a binary aluminosilicate compound intimately related in structure to sillimanite ($Al_2O_3 \cdot SiO_2$), a natural high-pressure, high-temperature mineral.[2] The mullite glass ceramic studied here falls into the general system SiO_2-Al_2O_3-B_2O_3-MO-R_2O, where M and R represent alkaline earth and alkali ions, respectively. This material is produced by heat treatment of the precursor glass. Chromium impurity ions, because of their large octahedral stabilization energy, only replace octahedral site Al^{3+}. The degree of distortion from perfect octahedral symmetry varies with the amount of crystallization that occurs during the heat treatment. Transmission electron microscopy and x-ray diffraction data reveal ordered regions of crystalline mullite ranging from 10 to 1000 Å in size[2] surrounded by a residual glassy matrix.

Previous work[1,2] has shown the mullites to have many properties characteristic of crystalline hosts such as a large average crystal-field strength (in excess of many crystalline materials) and strong R-linelike emission. However, they also exhibit behavior characteristic of low- or intermediate-field materials, generally resulting in $^4T_2$ emission. These materials also evince large inhomogeneous broadening in both phases.

In this paper we shall show that these properties can be attributed to the presence of both ordered high-field-site (HFS) and disordered low-field-site (LFS) Cr^{3+} ions, using evidence obtained from EPR, optical absorption, excitation, and emission spectra. The EPR spectrum is shown to contain the type of broad feature at $g_{\text{eff}} \approx 5$ which is always seen in Cr^{3+} doped glasses.[3,4] As in the experiments of Durville *et al.*,[5,6] this feature is shown to decrease with heat treatment. We shall prove that the broad spectrum originates from disordered LFS Cr^{3+} using a spin-Hamiltonian analysis. The optical excitation spectra allow us to distinguish between HFS and LFS Cr^{3+} behaviors. Finally, energy-transfer induced contributions are studied using the recently developed technique of saturation-resolved fluorescence (SRF) spectroscopy.[7]

II. ELECTRON PARAMAGNETIC RESONANCE

A. Experimental method and spectra

In order to isolate the behavior of LFS in the ceramic, a qualitative comparison is made between a glass ceramic and its precursor glass. A pair of samples, DNO/g glass and DNO/c mullite glass ceramic were chosen for the experiments (DNO is a Corning batch designation). DNO/g is a Corning proprietary, low-melting-temperature alumino-silicate glass doped with 0.05 wt. % Cr_2O_3. The glass ceramic is formed by annealing DNO/g for 2 h at 750 °C followed by 4 h at 800 °C.

EPR experiments were conducted with a Bruker ESR 200-D Spectrometer with a TE_{102} cavity operated at X band (9.42 GHz) with 100 kHz magnetic-field modulation. The samples were kept under vacuum in a sealed quartz tube. All measurements were performed at 15 K using an Oxford model ESR 9 cryostat. The same microwave power (50.00 mW) and instrument gain were used throughout the experiments.

The X-band first derivative EPR spectra of DNO/g and DNO/c (Fig. 1) have three features. The first and main feature is a broad asymmetric band at low-magnetic field with an effective g value of 5.36 for the precursor glass and 5.46 for the ceramic, respectively. This feature is always present in Cr^{3+}-doped insulating glasses and its

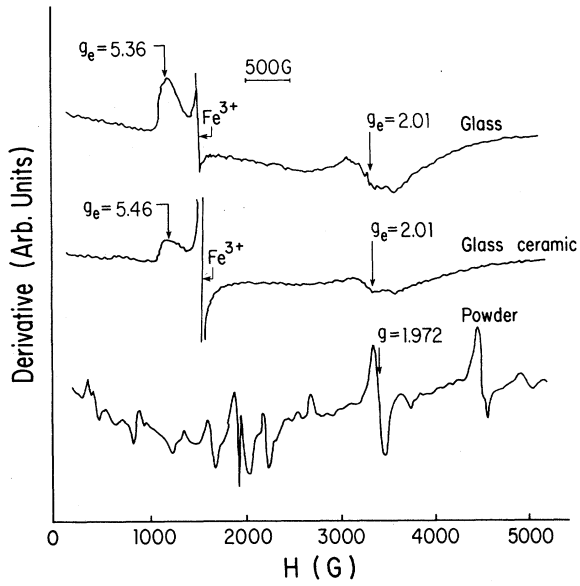

FIG. 1. EPR X Band first derivative spectra at 15 K of (upper) DNO precursor glass, (middle) DNO mullite glass-ceramic, and (lower) ruby powder (the many narrow peaks are the result of not grinding the powder fine enough).

presence in the ceramic points to ions in regions of disorder.[8] As can be seen from Fig. 1, the intensity of this signal is weaker in the ceramic than in the glass. The second feature is a relatively weak, asymmetric signal at high-magnetic field with $g_{\text{eff}} \approx 2$. Besides Cr^{3+}, impurities such as Fe^{3+} or exchange coupled pairs can contribute to this resonance. The third feature occurs at $g_{\text{eff}}=4.28$ and is typical of Fe^{3+} impurity ions in the raw materials.[3]

B. Analysis of the effective g factor

We now show that the broad feature at $g_{\text{eff}} \approx 5$ originates from Cr^{3+} ions at regions of disorder. A Cr^{3+} ion in a low-symmetry field can be described by the spin Hamiltonian[9]

$$\mathcal{H}=\beta\hat{H}\cdot\hat{g}\cdot\hat{\mathbf{S}}+D[\hat{\mathbf{S}}_z^2-\tfrac{1}{3}S(S+1)]+E(\hat{\mathbf{S}}_x^2-\hat{\mathbf{S}}_y^2)\ , \tag{1}$$

where D is an axial crystal-field parameter, E is an orthorhombic-field parameter, $\hat{\mathbf{S}}$ is the spin operator, and $\hat{g}$ is a second-rank tensor. Transforming (1) into coordinates[10] where the magnetic field is parallel to the x, y, or z axes yields

$$\begin{aligned}
&\mathbf{H}\|z \\
&\mathcal{H}_z=[g\beta H_z\hat{\mathbf{S}}_z+D\hat{\mathbf{S}}_z^2-\tfrac{1}{3}DS(S+1)]+\tfrac{1}{2}E(\hat{\mathbf{S}}_+^2+\hat{\mathbf{S}}_-^2)\ , \\
&H\|x \\
&\mathcal{H}_x=[g\beta H_z\hat{\mathbf{S}}_z+E\hat{\mathbf{S}}_z^2-\tfrac{1}{3}DS(S+1)] \\
&\quad+\tfrac{1}{4}(D-E)(\hat{\mathbf{S}}_+\hat{\mathbf{S}}_-+\hat{\mathbf{S}}_-\hat{\mathbf{S}}_+)+\tfrac{1}{4}(D+E)(\hat{\mathbf{S}}_+^2+\hat{\mathbf{S}}_-^2)\ , \\
&H\|y \\
&\mathcal{H}_y=[g\beta H_z\hat{\mathbf{S}}_z-E\hat{\mathbf{S}}_z^2-\tfrac{1}{3}DS(S+1)] \\
&\quad+\tfrac{1}{4}(D+E)(\hat{\mathbf{S}}_+\hat{\mathbf{S}}_-+\hat{\mathbf{S}}_-\hat{\mathbf{S}}_+)+\tfrac{1}{4}(D-E)(\hat{\mathbf{S}}_+^2+\hat{\mathbf{S}}_-^2)\ .
\end{aligned} \tag{2}$$

When (2) is diagonalized in the $|M_s\rangle$ basis, the $^4A_2$ state splits into two Kramer's doublets. In an external magnetic field these degenerate doublets split further. The energy eigenvalues, $W(D)$, of each of these four states can be obtained by solving the secular equations. Results of this procedure are plotted in Fig. 2.

The advantage of diagonalizing the transformed Hamiltonian (2) over treating the Zeeman term in (1) as a perturbation[10–12] is that the former places no restrictions on the values of D and E. Hence, the energy eigenvalues thus obtained are equally valid for the $D,E \gg h\nu$ and $D,E \sim h\nu$ cases.

If $D,E \gg h\nu$, the resonant transition can only occur within the Kramer's doublets (as seen Fig. 2), whereas if the magnitude of D and E is small, the transition can also occur between doublets. The parameters D and E are related to the zero-field splitting (Δ_{ZFS}) of the ground state $^4A_2$,

$$\Delta_{\text{ZFS}}=2(D^2+3E^2)^{1/2}\ , \tag{3}$$

and to the energy separation of the ground excited ($^4T_2$) states.[13] Zakharov estimated a 300 cm^{-1} Δ_{ZFS} from EPR measurements,[11] but the validity of this result was questioned by Zaripov,[14] who pointed out that such a splitting would lead to a sharp reduction in the spin-lattice relaxation time, making the resonance difficult to observe.[3] The results of Δ_{ZFS} (Refs. 15–18) studies indicate that D and E can be estimated to be much smaller than expected from Ref. 11. This suggests that both the intra–Kramer's and inter–Kramer's doublet transitions give rise to the $g \sim 5$ resonance.

For $E \neq 0$ (orthorhombic distortion), the Hamiltonian (2) contains the spin operators $\hat{\mathbf{S}}_+$ and $\hat{\mathbf{S}}_-$ which mix $|\frac{3}{2}\rangle$ with $|-\frac{1}{2}\rangle$ states and $|\frac{1}{2}\rangle$ with $|-\frac{3}{2}\rangle$ states, respectively. The eigenstates are then the linear combinations

$$|\bar{M}_s\rangle=c_1|M_s\rangle+c_2|M_{s\pm2}\rangle\ . \tag{4}$$

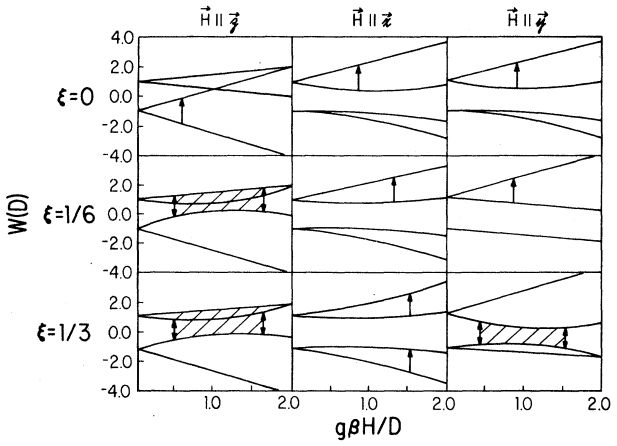

FIG. 2. Spin-Hamiltonian energy eigenvalues, $W(D)$, plotted as a function of $g\beta H/D$ for various orientations and amounts of axial and orthorhombic distortion (ξ). W has units of D. For $E=0$ the site symmetry is D_{4h} and the same energy-level diagram can be used for the $H\|x$ and $H\|y$ orientations.

The interaction of the spin system with an rf field applied perpendicular to H_0, gives rise to an additional term in the Hamiltonian, expressible as

$$\mathcal{H}_{(t)}=2g\beta H_R(\hat{\mathbf{S}}_x+\hat{\mathbf{S}}_y+\hat{\mathbf{S}}_z)\cos\omega t \ . \tag{5}$$

The transition matrix elements of $\mathcal{H}_{(t)}$ are nonzero within a doublet or between doublets in the basis of Eq. (4), which for different directions yields many possible values of the effective g factors, $g_{\text{eff}}=h\nu/\beta H$. However, as will be discussed later, the isolated discrete g values do not yield an observable resonance. The observable resonance, indicated by the shaded areas of Fig. 2, corresponds to the g factors

$$g_{\text{eff}}=2g\left[(1-\mu)^2+3\xi^2\mu^2\right]^{1/2} ,$$

$$g_{\text{eff}}=2g\left[\left[1-\frac{1+3\xi}{2}\mu\right]^2+3\left[\frac{1-\xi}{2}\mu\right]^2\right]^{1/2} ,$$

$$g_{\text{eff}}=g\left\{1+\left[\left[1+\frac{1-3\xi}{2}\mu\right]^2+3\left[\frac{1+\xi}{2}\mu\right]^2\right]^{1/2}-\left[\left[1-\frac{1-3\xi}{2}\mu\right]^2+3\left[\frac{1+\xi}{2}\mu\right]^2\right]^{1/2}\right\} , \tag{6}$$

where, $\xi=E/D$ and $\mu=D/g\beta H$. The g's above are second-rank tensors which can be calculated from second-order perturbation theory. However, because the splitting between the $^4A_2$ and $^4T_2$ states is large compared to the magnetic level splitting, we can make the approximation[10]

$$g=g_0-8\lambda/\Delta \ , \tag{7}$$

where g_0 is the free-electron g factor 2.0023 and λ is the spin-orbit coupling. An increase in Δ thus results in an increase in g. As will be explained below, Fig. 3 shows that a significant increase (>800 cm^{-1}) in the $^4A_2$-$^4T_2$ separation occurs after the heat treatment of the precursor glass.

In addition, increases in D or ξ also produce an increase in the Δ_{ZFS} given by (3). This dependence is also illustrated in Fig. 2. Transitions can only occur for values of D such that an X-band photon can bridge the energy gap. In the case of an ordered system such as ruby, with $D=0.19$ cm^{-1} and $E=0$, the resonances are sharp[19] and depend upon the orientation of the C_3 axis of the ruby crystal to H_0. For a crystallite system with no orientational preference, a powder pattern is expected.[13,20] The ruby powder spectrum (lower trace of Fig. 1) does not exhibit the broad feature at $g\sim5$ typically seen in glasses. In contrast, amorphous materials, because of random, inhomogeneous variations of D and ξ, have resonances which are considerably broadened. The broad regions which can be spanned by the X band are marked by the shadowed areas in Fig. 2. This is, of course, equivalent to a large spread in effective g values. The broad feature peaking at $g_{\text{eff}}=5.46$ observed in the ceramic is thus consistent with that observed for Cr^{3+} ions at regions of disorder.

The intensity and width of the resonance signal in glasses are dependent upon the distribution of D and ξ.[4] Since the local structure of most chromium sites in ceramics is relatively ordered, with a limited range of D and ξ values, they contribute little to the characteristic low-field signal. This is the reason why this signal, which is intense in glass, decreases upon crystallization.[8]

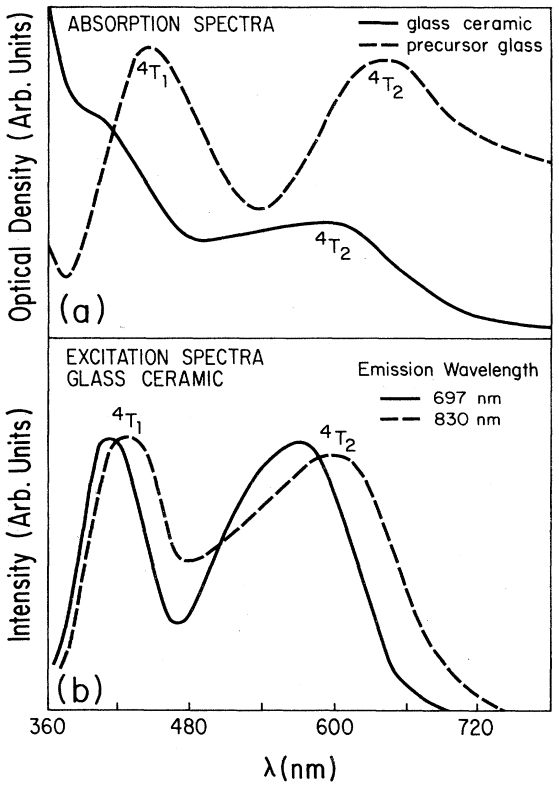

FIG. 3. (a) Absorption spectra of DNO mullite glass ceramic (solid curve) and precursor glass (dashed curve) showing the distinctive $^4T_1$ and $^4T_2$ absorption peaks of Cr^{3+}. (b) excitation spectra of Cr^{3+}: mullite glass ceramic for luminescence monitored at 697 nm (solid curve) and 830 nm (dashed curve).

The broad feature at $g_{\text{eff}}\approx5$ has been proven to result from Cr^{3+} at regions of disorder. The decrease in this low-field signal and its shift to larger effective g value have been shown to be consistent with the increased order or crystal-field strength, Δ, brought about by the annealing process. The residual presence of this peak in the ceramic allows us to conclude that Cr^{3+} remains to a small extent in disordered regions.

III. OPTICAL MEASUREMENTS

A. Absorption and excitation spectra

Absorption measurements of the glass and glass ceramic were performed at room temperature. The absorption spectra (Fig. 3) exhibit very broad $^4T_1$ and $^4T_2$ absorption bands of Cr^{3+}. From the peak positions we estimate an average Dq of 1710 cm^{-1} for the ceramic and 1590 cm^{-1} for the glass. The blue shift of the glass-ceramic absorption peaks with respect to those of the precursor glass shows that the annealing process, which increases the de-

gree of order, is accompanied by an increase in crystal-field strength. The average Dq noted for the glass ceramic makes it a very high ligand field material; for example, Dq is 1800 cm^{-1} for ruby, 1650 cm^{-1} for YGG (yttrium gadolinium garnet), and 1630 cm^{-1} for emerald.[21]

In order to ascertain the absorptions responsible for the R line and $^4T_2$ emissions, excitation spectra of individual features were measured. These data were obtained using a high-power tungsten halogen lamp/monochromator combination with a bandwidth of 15 nm and a photon counting system detector. Spectra were obtained at room temperature and 8 K; low temperatures were obtained by means of a closed cycle helium refrigerator.

The excitation spectra were found to be essentially temperature independent. The $^4T_2$ excitation peak (Fig. 3) of the glass ceramic, when monitored at 697 nm (R-line emission), is 540 nm. This spectrum represents the HFS, since only those sites emit R-line fluorescence. When monitored at 830 nm ($^4T_2$ emission) this excitation band expands toward a longer wavelength, becoming roughly 40 nm broader than the corresponding excitation band for R-line emission; the low-energy excitation edge extends well past the R-line region. The peak now occurs at 600 nm, indicating that the ions responsible for this $^4T_2$ luminescence have a lower average ligand field strength than those which emit R lines. It is reasonable, therefore, to assume that this peak shift is due to the additional presence of a LFS excitation peak. Since the HFS can contribute to this emission through energy transfer (see Fig. 4) the excitation band for 830-nm emission is really a convolution of HFS and LFS contributions, with the actual LFS peak lying even further to the red. By comparing the net area increase with the area of the entire band, we estimate that roughly 12% of the Cr^{3+} ions lie in LFS. The $^4T_1$ excitation peak shows similar behavior, peaking at 400 and 420 nm for 697- and 830-nm emissions, respectively.

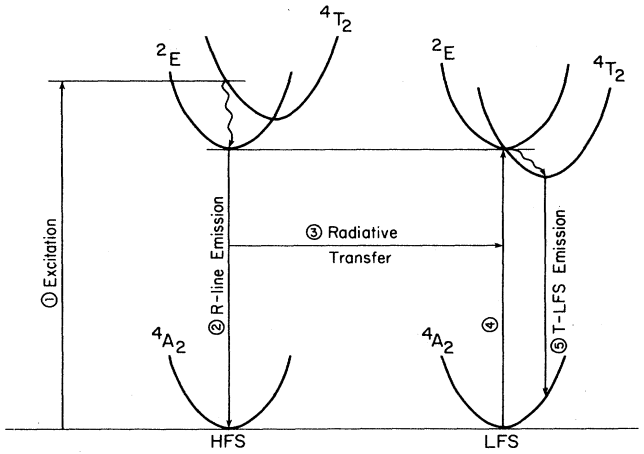

FIG. 4. Energy-level diagram of HFS and LFS Cr^{3+} demonstrating the energy-transfer mechanism. The lowest-lying, and therefore radiating, excited state is the ^2E level for HFS ions whereas it is the $^4T_2$ level for LFS ions. A HFS ion excited by the laser pulse will emit R-line photon which can be subsequently absorbed through a $^4A_2$-$^4T_2$ transition of a LFS ion. The excited LFS ion can then relax back to the ground state via the Stoke's shifted luminescence denoted T-LFS emission.

In short, monitoring the R-line emission yields a HFS spectrum similar to that of high-field crystalline materials such as ruby, while monitoring the $^4T_2$ emission yields a spectrum such as found for common glasses. Comparison of the absorption and excitation data suggests that the absorption spectrum of the glass ceramic is actually a convolution of the absorptions of various sites, representing a wide range of ligand field strengths. The low-energy edge of the absorption spectrum therefore contains significant contributions from LFS for which the Stokes-shifted $^4T_2$ state is the lowest-lying (Fig. 4), and therefore radiating, level.

B. Emission spectra

The previous data suggest that the ratio of high-field to low-field emission depends on what region of the $^4T_1$ or $^4T_2$ absorption is excited.[22] Emission spectra were taken at various excitation wavelengths to test this hypothesis. Both pulsed and cw measurements were done because they reflect different dynamical situations.

Time-resolved fluorescence spectra were excited by an Nd:YAG (yitrium aluminum garnet) laser or YAG-pumped dye laser. At long-delay times mostly R-line emission (3.5-ms lifetime) around 700 nm is observed whereas at short-delay times the short-lived ($\approx$40 μs lifetime) broadband $^4T_2$ emission (centered near 800 nm) becomes more apparent (Fig. 5). cw spectra were obtained

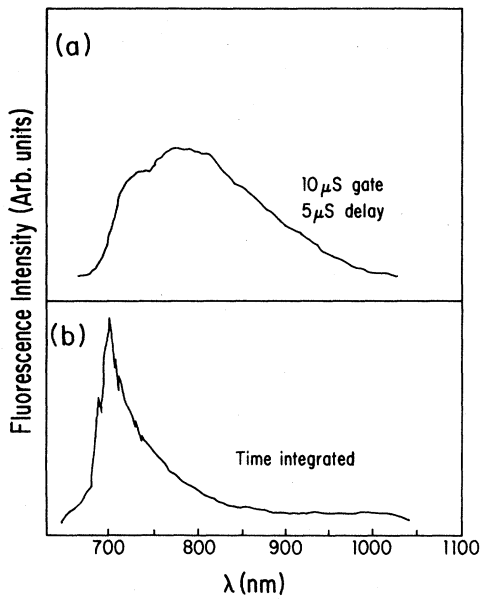

FIG. 5. Pulsed room-temperature luminescence of Cr^{3+}: mullite DNO glass-ceramic under 532 nm excitation. (a) is a superposition of HFS R-line emission and a broad $^4T_2$ emission containing LFS contributions. This spectrum was obtained using a narrow integration gate with a minimal delay after the excitation pulse to maximize the short-lived $^4T_2$ contribution (b) shows a typical R-line emission from the ^2E level of HFS Cr^{3+}. The long tail extending to 1 μm originates from LFS $^4T_2$ emission activated through radiative energy transfer. This spectrum was obtained with a wide integration gate to average all decay components. The predominance of the R-line feature indicates that most of the Cr^{3+} ions lie in HFS.

using the excitation spectra apparatus. These spectra resemble the time-integrated spectra obtained with the pulsed system, showing mostly R-line emission and a long tail extending past 1 μm (Fig. 6).

The fluorescence spectra contain several notable features. The $^4T_2$ emission is site selective, as is demonstrated by plotting the peak wavelength as a function of excitation wavelength (Fig. 7). This indicates a large inhomogeneous broadening of the LFS due to disorder.[23,24] That this emission is still observed for excitation energies below the ^2E resonance provides further evidence of LFS. Furthermore, residual broadband emission is still observed at 8 K, indicating a LFS origin (Fig. 6) for this fluorescence; at this temperature any $^4T_2$ emission from intermediate field sites, due to a thermal equilibrium between the ^2E and $^4T_2$ levels, should be frozen out. The ratio of HFS to LFS emission observed agrees with the results of Sec. III A, namely, excitation in the HFS region of Fig. 3 yields less broadband emission than does excitation at the LFS side. Finally, the overlap of the LFS absorption with the HFS R-line emission leads to radiative energy transfer between these species. Three types of emission are therefore possible: R-line emission from HFS, $^4T_2$ emission from those LFS directly excited by the laser (denoted D-LFS for "directly excited LFS"), and a secondary $^4T_2$ emission from those LFS excited through absorption of HFS R-line emission (denoted T-LFS for "energy-transfer excited LFS"). The shape of the curve in Fig. 7 reflect the presence of these three emissions. As the excitation wavelength moves from 532 to 770 nm, the subset of ions directly excited goes from higher to lower field. For excitation energies below the ^2E level, only D-LFS emission is present and the peak wavelength shifts rapidly with excitation wavelength, whereas for excitation energies in excess of the ^2E level, this emission is superimposed on that of the HFS and T-LFS. Therefore, over this region the peak wavelength shifts slowly with excitation wavelength.

C. Saturation-resolved fluorescence spectroscopy

The strength of the HFS emission makes it impossible to isolate the other emissions by time resolved or phase resolved techniques. However, the D-LFS emission can be extracted using the SRF technique. In this procedure, two laser beams are counter-propagated collinearly through the sample, very close to the surface. The first beam "saturates" the radiative energy transfer from HFS to LFS by saturating the absorption of the HFS donor ions, or alternatively, by saturating the $^4T_2$ absorption of the LFS acceptor ions at the same wavelength as the HFS emission. The second, or probe, beam can therefore only increase the D-LFS emission. Because the "saturated" T-LFS emission remains constant, the D-LFS emission can be isolated by subtracting the spectrum excited by the saturating beam only from the spectrum excited by both beams. This is done by taking consecutive one- and two-beam spectra. An alternate method is to use a pulsed probe laser, cw saturating laser, and a two-channel boxcar integrator. The first channel records the signals when both beams are incident on the sample while the second monitors the luminescence when only the saturating beam is present. Operating in difference mode then yields the D-LFS emission directly. The luminescence from the saturated region is isolated by a mask designed to eliminate background emissions resulting from laser scatter and long-range radiative transfer. Furthermore, great care is taken to ensure the spatial overlap of the two beams. The experiments are performed at room temperature to allow laser excitation over a broader spectral region than would be possible at low temperature.

The luminescence excited solely by the saturating beam is seen in trace 2 of Fig. 8. Introduction of the second beam (trace 1 of Fig. 8) clearly results in an enhancement

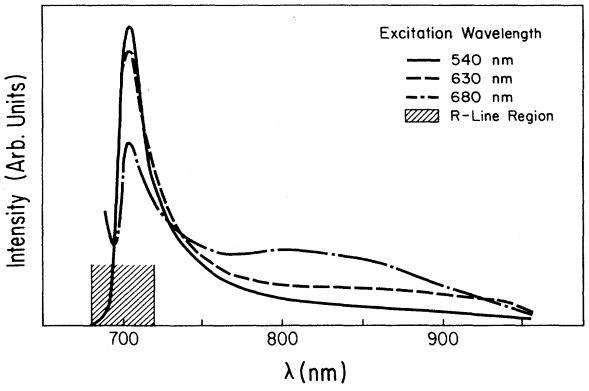

FIG. 6. cw luminescence of Cr^{3+}: mullite glass-ceramic DNO at 8 K under (1) 540-nm, (2) 630-nm, (3) 680-nm excitation.

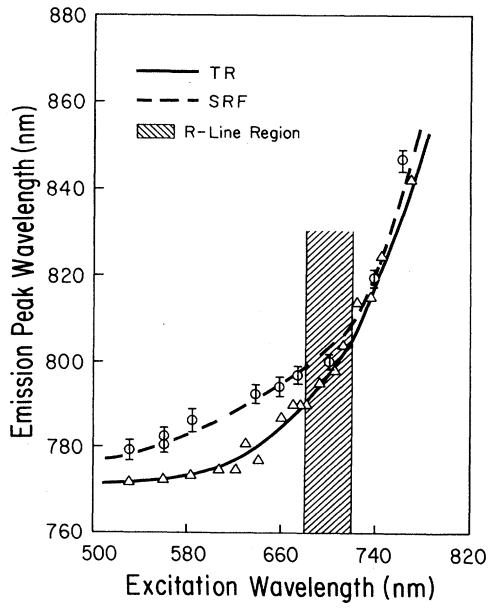

FIG. 7. Peak emission wavelength of Cr^{3+}: mullite glass ceramic plotted as a function of excitation wavelength. The solid curve represents the peak positions of conventional time-resolved spectra taken with a 10-μs gate and 5-μs delay at room temperature. The dashed curve represents the peak positions of the D-LFS obtained by SRF spectroscopy.

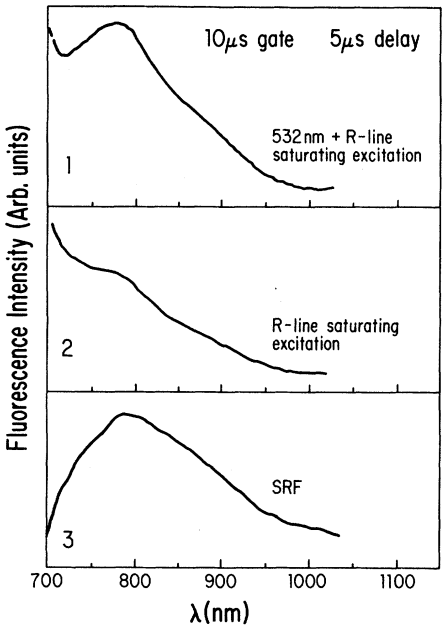

FIG. 8. SRF spectra obtained under (1) R-line resonant saturating beam plus 532 nm probe beam, (2) saturating beam only. The D-LFS emission, trace (3), is obtained by taking the difference of traces (1) and (2), and has a profile typical of Cr^{3+}: glasses.

of the $^4T_2$ emission. The D-LFS emission (trace 3 of Fig. 8), obtained by taking the difference of traces 1 and 2, is seen to have a profile typical of glasses. The peak wavelength of this emission is plotted in Fig. 7 as a function of excitation wavelength. For excitation wavelengths shorter than the R lines, the D-LFS emission is seen to peak at longer wavelengths than the unresolved emission. In addition to the D-LFS component, the unresolved emission contains strong R-line contributions at shorter wavelength and weaker T-LFS contributions at longer wavelength. This results in an overall blue shift with respect to the D-LFS emission. The D-LFS luminescence is also seen to be site selective. Because the R-line emission, and hence the T-LFS emission occurs at fixed wavelength, the site selectivity observed in the overall fluorescence is due to the D-LFS component.

IV. CONCLUSION

The average crystal field of these materials is actually higher than that of alexandrite yet the broad optical and EPR signals resemble those found in glasses. This anomalous behavior can be accounted for by a model in which the degree to which Cr^{3+} relaxes into ordered HFS is dependent upon the heat treatment. Those ions in ordered HFS show excitation peaks and R-line emission similar to high-field materials such as ruby. The predominance of R-line emission in the materials tested suggests that most of the ions belong to this category. Those ions in disordered LFS contribute to the broad low-field feature at $g_{\text{eff}} \approx 5.46$ noted in the EPR spectrum, the low-energy edge of the $^4T_1$ and $^4T_2$ absorption peaks, excitation peaks for $^4T_2$ emission which are red shifted with respect to the excitation peaks for R-line emission, and broad $^4T_2$ emission which shows a significant degree of site selectivity and which can be excited at energies below the ^2E level.

The observation of energy transfer from ordered high-field regions to disordered low-field regions is most interesting. Equally intriguing is the result that this energy transfer can be "saturated." This allows us to study the D-LFS luminescence in isolation from the other emissions, revealing a profile and site selectivity typical of disordered materials.

Inasmuch as the glass ceramic consists of crystalline regions of various size within a glassy matrix, it is natural to assume that there exists a transitional region bridging the two phases. For example, Cr^{3+} at the interfaces surely encounter a smaller crystal field. Additionally, the transitional region cannot be excessively sharp as it is produced by a statistical process. Such a region would possess a very interesting structure. It is plausible that the disordered LFS substantiated in this paper represent this transitional region. The percent crystallinity, the size and surface to volume ratio of the microcrystals, and the amount of Cr^{3+} migration are all governed by the thermal history of the sample. The degree of low-field behavior should therefore depend on the heat treatment.

ACKNOWLEDGMENTS

The authors would like to express their thanks to Dr. Douglas W. Hall for providing samples and to Dr. Donald S. McClure, Dr. Marvin J. Weber, and Dr. Hall for useful discussions and suggestions. This research was supported by U.S. Department of Energy (DOE) Contract No. DE-FG-09-87ER45291.

*Also at the Department of Physics, University of Wisconsin, Madison, WI 53706.

[1]L. J. Andrews, A. Lempicki, and B. C. McCollum, J. Chem. Phys. **74**, 5526 (1981).

[2]G. H. Beall, D. R. Cole, D. W. Hall, H. J. Holland, J. W. H. Schreus, M. Edwards, R. Gillies, and A. Lempicki, U.S. Dept. of Energy report, 1987 (unpublished).

[3]J. Wong and C. A. Angell, *Glass: Structure by Spectroscopy* (Marcel-Dekker, New York, 1976), Chap. 9.

[4]D. L. Griscom, J. Non-Cryst. Solids **40**, 211 (1980).

[5]F. Durville, B. Champagnon, E. Duval, and G. Boulon, J. Phys. Chem. Solids **46**, 701 (1985).

[6]F. Durville, B. Champagnon, E. Duval, G. Boulon, F. Gaume, A. F. Wright, and A. N. Fitch, Phys. Chem. Glasses **25**, 126 (1984).

[7]H. Liu, R. Knutson, and W. M. Yen (unpublished).

[8]C. Blanchard, A. Deville, A. Boukenter, B. Champagnon, and E. Duval, J. Phys. (Paris) **47**, 1931 (1986).
[9]R. J. Landry, J. T. Fournier, and C. G. Young, J. Chem. Phys. **46**, 1285 (1967).
[10]F. Gan, H. Deng, and H. Liu, J. Non-Cryst. Solids **52**, 135 (1982).
[11]B. K. Zakharov *et al.*, Fiz. Tverd. Tela **7**, 1571 (1965) [Sov. Phys. Solid State **7**, 1267 (1965)].
[12]R. H. Sands, Phys. Rev. **99**, 1222 (1955).
[13]A. Abragam and B. Bleaney, *Electron Paramagnetic Resonance of Transition Ions* (Dover, New York, 1970), pp. 200 and 401.
[14]M. M. Zaripov, Fiz. Tverd. Tela **7**, 3666 (1965) [Sov. Phys. Solid State **7**, 2960 (1966)].
[15]R. M. Macfarlane, J. Chem. Phys. **47**, 2066 (1967).
[16]L. Grabner, S. E. Stokowski, and W. S. Brower, Jr., Phys. Rev. B **2**, 590 (1970).
[17]G. Burns *et al.*, Phys. Rev. **167**, 314 (1968); Phys. Lett. **23**, 56 (1966).
[18]H. Liu, K. Lim, W. Jia, E. Strauss, W. M. Yen, A. M. Buoncristiani, and C. E. Byvik, Opt. Lett. **13**, 931 (1988). Here the variation of the Δ_{ZFS} with the $^4A_2$-$^4T_2$ energy separation was found to be small. Recent work on Cr^{3+}:$LiNbO_3$, which has a rhombic structure, also shows that the variation of the Δ_{ZFS} with stress is small.
[19]G. R. Sinclair *et al.*, J. Magn. Reson. **57**, 228 (1984).
[20]D. L. Griscom, J. Non-Cryst. Solids **31**, 241 (1978).
[21]D. L. Wood, J. Ferguson, K. Knox, and J. F. Dillon, Jr., J. Chem. Phys. **39**, 890 (1963).
[22]W. M. Yen, in *Physics and Chemistry of Materials with Low-Dimensional Structure, Series C, Molecular Structure,* edited by I. Zschokke (Reidel, Boston, 1986), p. 53.
[23]M. J. Weber, in *Laser Spectroscopy of Solids,* Vol. 49 of *Topics in Applied Physics,* edited by W. M. Yen and P. M. Selzer (Springer-Verlag, New York, 1981), p. 189.
[24]A. J. Wojtowicz and A. Lempicki, J. Lumin. **39**, 189 (1988).